Numerical Simulation of the Multi-Roller Skew Tandem Rolling of Unequal Wall Thickness Hollow Stepped Shafts

Yexin Huang[1,2], Xuedao Shu[1,2,*], Song Zhang[3], Zewei Cen[1,2], Haijie Xu[1,2], Zixuan Li[1,2], Yingxiang Xia[1,2], Pater Zbigniew[4] and Bulzak Tomasz[4]

[1]*Faculty of Mechanical Engineering and Mechanics, Ningbo University, Ningbo 315211, China*

[2]*Zhejiang Provincial Key Laboratory of Part Rolling Technology, Ningbo 315211, China*

[3]*College of Mechanical and Automotive Engineering, Ningbo University of Technology, Ningbo 315211, China*

[4]*Faculty of Mechanical Engineering, Lublin University of Technology, Nadbystrzycka Str. 36, 20-618 Lublin, Poland*

Abstract: This paper proposes a multi-roll skew rolling forming process to address the slow forming speed of large-section shrinkage for aviation turbine shafts. Using Simufact Forming software, simulations were conducted on the GH4169 turbine shaft blank, analyzing the variations in stress, strain, and temperature fields during the forming process of a hollow shaft component with an initial wall thickness of 6mm. Additionally, we further explored the intrinsic relationship between the initial wall thickness and the depth of the concave center at the end of the workpiece. The results indicate that after multi-field coupling effects, the metal deformation of the workpiece gradually accumulates along the axial direction, reaching a peak after achieving the maximum reduction, while displaying a trend of decreasing from the outside to the inside. Additionally, there is a positive correlation between the depth of the concave center at the end of the workpiece and the initial wall thickness; as the amount of metal involved in the deformation increases, the depth of the concave center also intensifies. These findings provide an important theoretical basis for achieving flexible rolling formation of turbine shafts.

Keywords: Aviation turbine shaft, Multi-roller skew tandem rolling, Initial wall thickness, Concavity depth.

INTRODUCTION

Aviation turbine shafts are a critical component of aircraft engines [1], operating under demanding conditions marked by high temperatures and complex loading scenarios. Consequently, it is vital to select high-temperature alloys that exhibit outstanding mechanical properties and corrosion resistance. One such alloy is the nickel-based alloy GH4169 [2]. To meet functional requirements, aviation turbine shafts often incorporate design features such as substantial cross-sectional reduction ratios and uniform inner diameters.

Currently, the primary forming processes for turbine shafts include die forging and wedge rolling. Wang *et al.* [3] noted that using the axial elongation forging method within the die forging process results in poor dimensional accuracy and low work efficiency for the forged parts. Although combining local elongation of the rod section with local forging of the flange can enhance certain properties, this approach often leads to a significant decline in overall performance. Tan *et al.* [4] conducted experiments on the large cross-sectional reduction rolling of TC4 shaft components, finding that their simulation results closely aligned with numerical data. However, the limitations of rolling mill size pose

challenges for achieving the rolling of aviation turbine shafts. Pater *et al.* [5] performed an in-depth study on producing long shaft components, slender preforms, and hollow shafts with mandrels using a three-roll skew rolling process. Their findings revealed minimal discrepancies between simulation data and experimental results, with no internal void defects in the formed parts, resulting in high dimensional accuracy. Shu *et al.* [9] proposed a method that combines piercing rolling with three-roll rolling for the manufacture of hollow shafts, which was validated using Simufact Software. Nonetheless, due to roll gap limitations, achieving the required large radial cross-sectional reduction in a single operation remains challenging. Zhang *et al.* [15] combined constitutive models, microstructure evolution, hot processing maps, and TRSR simulations/experiments, finding that the simulation results for wall thickness variations align well with the actual measurements. This demonstrates the feasibility of forming hollow stepped shafts from high-strength Al–Zn–Mg–Cu alloy using the TRSR process. Chen *et al.* [17] established speed and tension models based on the skew tandem rolling process, successfully rolling titanium alloy seamless tubes. Additionally, Chen *et al.* [19] demonstrated the feasibility of an integrated cross-rolling forming process by analyzing relevant parameters in their study. While these studies provide valuable methods and theoretical support for the precise forming of large cross-section reduction shaft components, they do not systematically explore the relationship between varying initial wall

*Address correspondence to this author at the Faculty of Mechanical Engineering and Mechanics, Ningbo University, Ningbo City 315211, China; E-mail: shuxuedao@nbu.edu.cn

thicknesses and the formation of hollow stepped shaft ends.

This paper introduces an improved three-roll skew rolling forming process that connects two sets of three rollers to effectively reduce the diameter of the workpiece by adjusting the roll gap. The feasibility of rolling hollow stepped shafts at large cross-sectional reduction rates is investigated through simulation. The study examines the influence of the initial wall thickness of the workpiece on the end forming quality achieved at these reduction rates. This novel process aims to enhance both forming precision and process efficiency, offering a theoretical foundation for the flexible rolling of aerospace turbine shafts.

1. MODEL ESTABLISHMENT AND VERIFIED

1.1. Coordination Relationship of Rolling Speeds

To prevent issues such as twisting or breakage of the workpiece during the continuous rolling process, a speed coordination formula has been developed based on the size parameters and rotational speeds of the leading rollers. This formula aims to minimize defects during rolling [20]. As illustrated in Figure **1**, the roller speed is decomposed into radial and axial velocity components. In practical rolling experiments, a slip phenomenon often occurs between the die and the workpiece; therefore, the representation of the velocity components is as follows:

$$
\begin{cases}
v_{Rt1} = \dfrac{\eta_{T1}\pi D_{R1}\omega_1 \cos\alpha_1}{60} \\[2mm]
v_{Ro1} = \dfrac{\eta_{o1}\pi D_{R1}\omega_1 \sin\alpha_1}{60} \\[2mm]
v_{Rt2} = \dfrac{\eta_{T2}\pi D_{R2}\omega_2 \cos\alpha_2}{60} \\[2mm]
v_{Ro2} = \dfrac{\eta_{o2}\pi D_{R2}\omega_2 \sin\alpha_2}{60}
\end{cases}
\tag{1}
$$

where: η_{T1} and η_{o1} stand for the axial slip coefficient and tangential slip coefficient for the leading skew rolling mill. η_{T2} and η_{o2} stand for the axial slip coefficient and tangential slip coefficient for the trailing skew rolling mill. α_1 and α_2 stand for the feed angles of the skew rolling mills, in degrees. v_{Rt1} and v_{Ro1} stand for the axial and tangential velocity components of the leading skew rolling mill, in mm/s. v_{Rt2} and v_{Ro2} stand for the axial and tangential velocity components of the trailing skew rolling mill, in mm/s. D_{R1} and D_{R2} stand for the maximum diameters of the leading and trailing rolls, in mm. n_{r1} and n_{r2} stand for the rotational speeds of the leading and trailing rolls, in r/min.

Under ideal conditions, the axial exit velocity at both ends of the middle section of the workpiece during the rolling process should equal the axial entry velocity. Concurrently, the radial exit velocities at both ends should correspond with the radial entry velocities.

Achieving this coordination can significantly minimize deformation defects throughout the rolling process, thereby enhancing the overall quality and forming accuracy of the workpiece. This relationship can be mathematically represented as follows:

$$
\frac{\omega_1}{\omega_2} = \frac{\eta_{T2}D_{R2}\cos\alpha_2}{\eta_{T1}D_{R1}\cos\alpha_1}
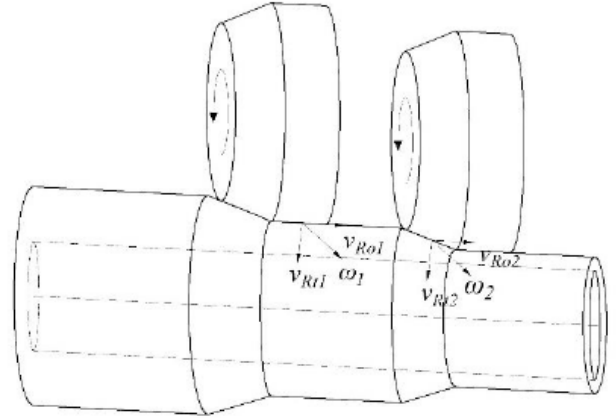\tag{2}
$$

Figure 1: Skew rolling speed component diagram.

1.2. Finite Element Model Parameter Setting

The finite element model of the skew tandem rolling process primarily consists of the front skew roller, the rear skew roller, the pusher, the fixed ring, the mandrel, and the workpiece, as shown in Figure **2**. The presence of the core rod is essential to ensure the stability of the formed part and the consistency of the inner diameter.

The workpiece has dimensions of $\Phi 50 \times 140$ mm with a wall thickness of 6 mm, and a sheet mesh is employed for grid division. The grid is refined in the radial direction, resulting in a total of 43,860 elements. The roller parameters, calculated from the equations mentioned above, are summarized in Table **1**.
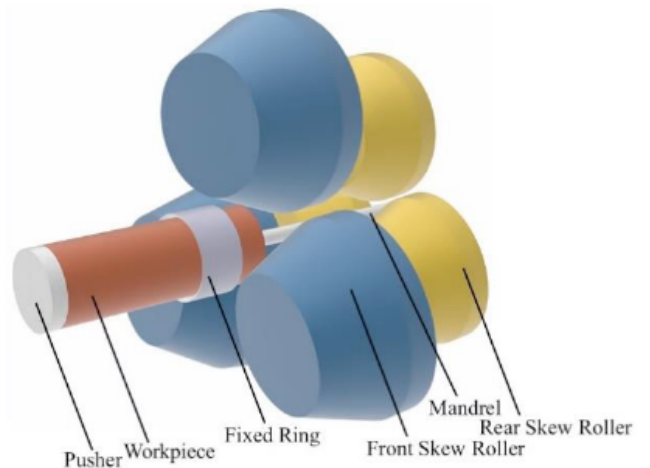

Figure 2: Skew rolling forming process model.

Table 1:   Roller Size and Speed Parameters

| Parameter	Reduction Section Length/mm	Finish Section Length/mm	Maximum Diameter of the roller/mm	Roller Speed/rad·min^{-1}
The front skew roller	70	20	130	30
The rear skew roller	54	15.5	100	39

1.3. Boundary and Initial Condition Settings

In the skew tandem rolling process, the workpiece is treated as a plastic material, while the rest of the model is considered a rigid body. The workpiece experiences significant cross-sectional reduction in a high-temperature environment, classifying it under large plastic deformation. Consequently, a shear friction model is employed to account for the friction between the rollers and the workpiece. According to the literature [21], a higher friction coefficient between the rollers and the workpiece facilitates the rolling process. Therefore, in the simulation analysis, the friction coefficient between the workpiece and the rollers is set to 0.9, while the friction coefficient between the workpiece and other components of the model is set to 0.1. This configuration aims to minimize the influence of other components on the rolling forming process, thereby allowing for a more accurate simulation and optimization of the rolling results.

During the rolling process, the workpiece experiences an increase in temperature due to plastic deformation and frictional contact with the rollers [22]. This temperature rise occurs primarily because metals generate heat during plastic deformation, and the frictional force further elevates the temperature of the workpiece. In addition to the internal heat generated within the workpiece, significant heat transfer also takes place between the workpiece, its surrounding environment, and other model components. To accurately simulate this process, the following temperature parameters were established for the simulation experiment: workpiece temperature at 1050°C, other model components at 150°C, and environmental temperature at 20°C. Furthermore, to better reflect thermal transfer characteristics, the thermal transfer coefficients were defined as follows: the coefficient between the workpiece and the environment is set to 50 W/(m²·K), while the coefficient between the workpiece and the molds is set to 20,000 W/(m²·K).

These detailed settings enable an effective simulation of the heat transfer behavior during the rolling process, allowing for an in-depth analysis of temperature changes in the workpiece and their impact on forming performance. This simulation not only enhances understanding of thermal management during the rolling process but also aids in optimizing production processes, ultimately improving forming efficiency and product quality.

The simulation results compared with the target shaft shape are shown in Figure **3**, demonstrating that the overall shape and dimensions meet the design requirements, On the longitudinal section of the workpiece, evenly select 8 sampling points along the axial direction in the first reduction section, and also evenly select 8 sampling points in the second reduction section. The variance of the circumference diameter in the first reduction is 0.00132, the variance of the circumference diameter in the second reduction is 0.00561. During the forming process, the workpiece did not exhibit any defects such as twisting, fracture, or collapse, indicating that the inclined continuous rolling
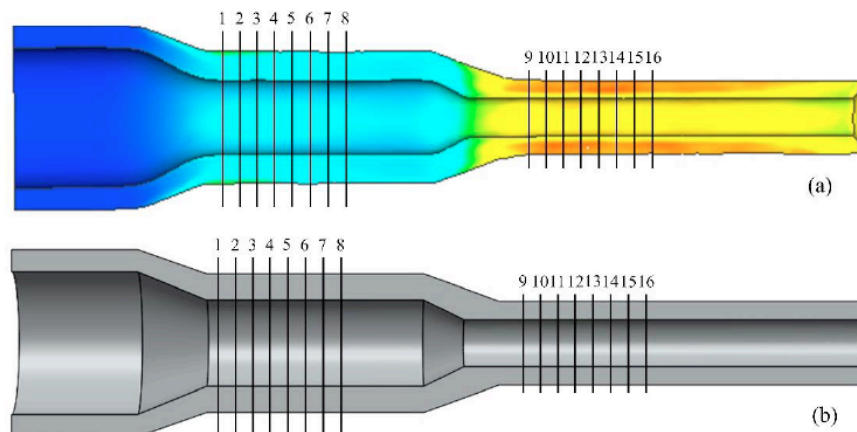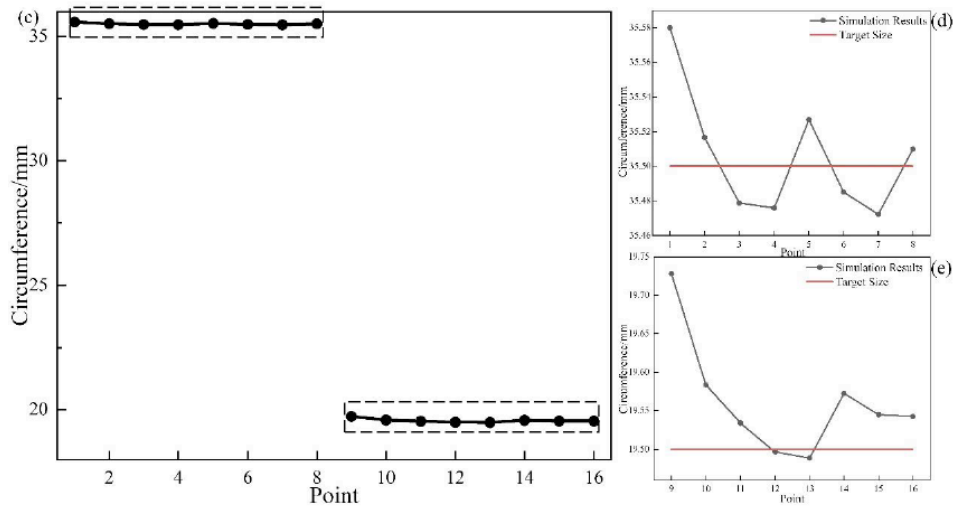
Figure 3: (**a**) Simulation Shape; (**b**) Target Axial shape; (**c**) The Circumference of Simulation Results; (**d**) Comparison of the circumference of simulation results with the expected target dimensions from Point 1 to 8; (**e**) Comparison of the circumference of simulation results with the expected target dimensions from Point 9 to 16.

integration forming process has excellent forming performance. This process effectively achieves the design objectives and ensures product quality.

2. FINITE ELEMENT RESULTS AND ANALYSIS

2.1. Wall Thickness of the Formed Part

During the skew tandem rolling process, the workpiece undergoes an increase in wall thickness in the radial direction during the initial diameter reduction. Following this initial rolling, the wall thickness fluctuates around 7.8 mm. At the onset of the second diameter reduction, the wall thickness reaches its maximum before gradually thinning throughout the rear rolling stages. The overall trend of wall thickness variation is depicted in Figure **4**, clearly illustrating the impact of different rolling stages on wall thickness.
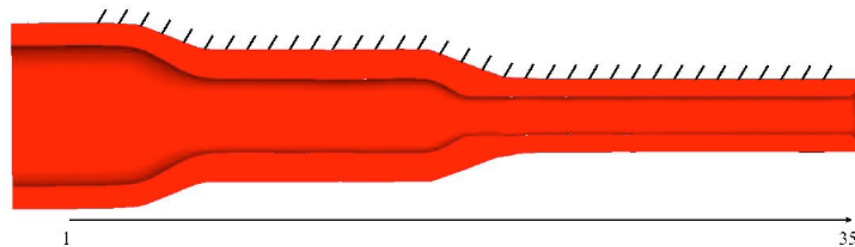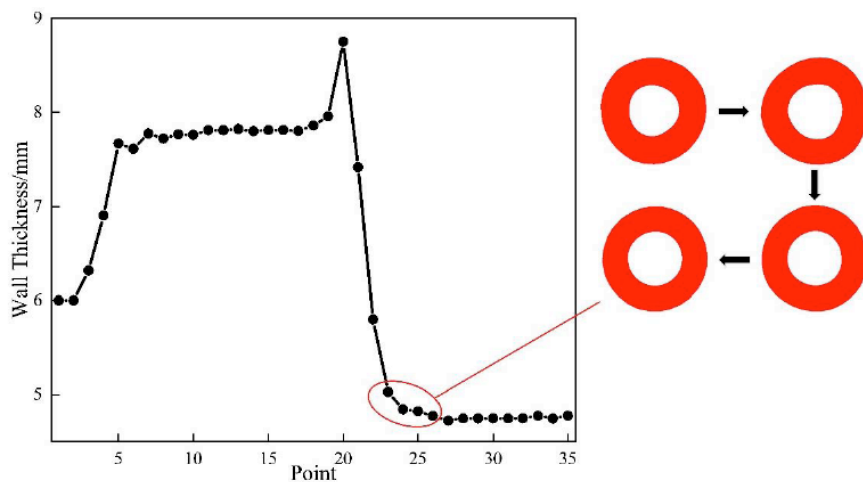
Figure 4: (**a**) Sampling points of the cross-section of the workpiece; (**b**) The variation law of the overall wall thickness of the workpiece and the part of the cross-section changes.

2.2. Stress-Strain Analysis

Figure **5** illustrates the distribution of equivalent plastic strain, with the rolling process divided into four stages: Stage 1 - Front Roller Bite Phase, Stage 2 - Rear Roller Bite Phase, Stage 3 - Synchronization Rolling Phase, and Stage 4 - Completion Phase. In Stage 1, the end of the workpiece initially contacts the diameter reduction section of the roller, where the metal in the contact area experiences triaxial compressive stress, causing the plastic strain rate to peak. The metal flow exhibits radial and circumferential compression, accompanied by axial elongation. During this stage, the shape of the workpiece undergoes significant deformation, transitioning from circular to circular-triangular in the contact area before returning to a circular shape under the influence of the roller's finishing section. Throughout this process, the contact and deformation trends in the rear roller align with those of the front roller, suggesting that adjusting the roller speeds appropriately can help stabilize the rolling process.

During the rolling process, the metal in the contact area remains under triaxial compressive stress, maintaining a high plastic strain rate. This stress state leads to radial and circumferential compression, along with axial elongation, resulting in the continuous accumulation of deformation along the axial direction as the diameter reduction progresses. After the second diameter reduction, the plastic strain reaches a maximum value of 8.84. The plastic strain distribution within the material decreases gradually from the outer surface to the core. This pattern primarily arises from the intense friction between the workpiece and the rollers, which induces dense flow in the circumferential direction. Consequently, the outer regions of the workpiece experience higher strain, while the inner regions experience lower strain. Such a strain distribution may give rise to adverse residual stresses in the formed shaft.

Figure **6** depicts the distribution of equivalent plastic stress across the cross-section of the formed workpiece. During the diameter reduction process, the significant decrease in the workpiece size generates substantial deformation resistance. As a result, the maximum equivalent plastic stress concentrates in the diameter reduction area, where the roller contacts the workpiece, reaching up to 581 MPa. In the second diameter reduction, the core of the workpiece restricts the radial flow of metal, creating localized high-stress regions at the inner wall of the contact zone between
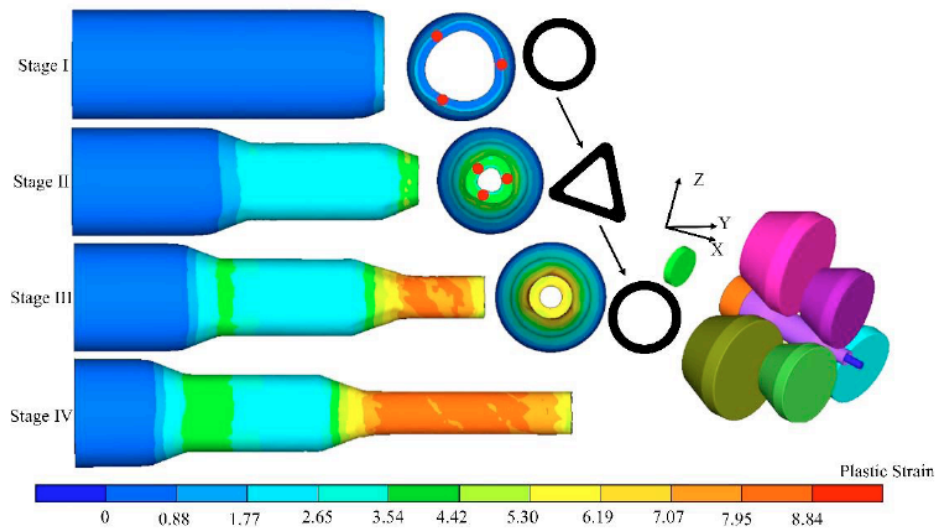

Figure 5: Forming process and strain field distribution of workpiece.
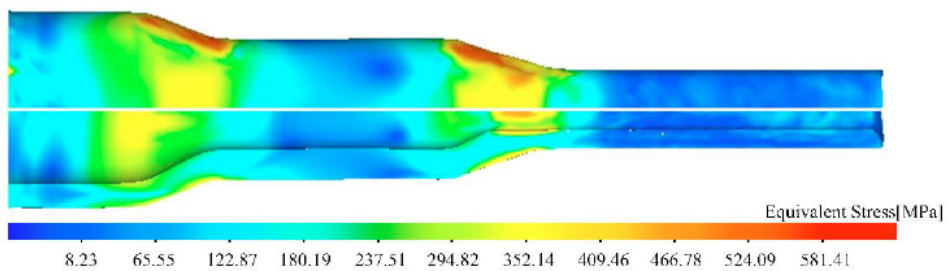

Figure 6: Equivalent stress field distribution.

the rollers and the workpiece. After the diameter reduction, some residual stress values fall below 122 MPa.

2.3. Temperature Field Analysis

As shown in Figure **7**, the selected points on the external, middle, and internal layers of the workpiece and their temperature variations. At 3 seconds, the selected point begins to make contact with the front roller, leading to a temperature increase of approximately 80°C, primarily due to deformation heat. The external point shows a relatively minor trend in temperature change, which can be attributed to the simultaneous generation of friction heat and deformation heat at the contact point with the roller, along with heat transfer. Additionally, the lower rotational speed of the front roller limits the extent of temperature rise in the external region. At 9 seconds, the selected point starts to contact the rear roller. Initially, when the external point engages with the reducing section of the rear roller, a temperature drop occurs, followed by a subsequent rise due to the influence of friction heat and deformation heat. This increase continues until the point disengages from the finishing section of the rear roller. After 9 seconds, the temperature of the middle point begins to rise, peaking around 12 seconds before declining. This temperature behavior is linked to the secondary reduction process, which effectively thins the wall thickness. During this phase, the middle layer experiences radial forces from both the external roller and the internal mandrel, with deformation heat serving as the primary driving factor. At approximately 11 seconds, the internal point experiences a rapid temperature drop upon contact

with the mandrel. Analyzing Figure 3 reveals fluctuations in wall thickness between points 26 and 33, resulting in the formation of voids. This phenomenon primarily arises from the presence of the mandrel, which leads to a mismatch in the radial flow velocities of the metal during the secondary reduction process, ultimately creating voids. This observation aligns with Bulzak's study on the rolling of hollow shafts using a mandrel to stabilize the inner diameter, where similar voids were noted.

3. DEFECT PROBLEM

3.1. Mechanism and Control of End Concave Center Generation

After undergoing a second reduction rolling process, significant concavity was observed at the ends of the workpiece. This phenomenon can be attributed to the radial variation in deformation within the contact area between the rollers and the workpiece. Typically, deformation decreases gradually from the outer to the inner region, resulting in an uneven distribution that contributes to the concavity at the ends of the workpiece. In contrast to the mandrel, the rollers act as the active components, exerting radial compression and axial elongation on the flow of the external metal of the workpiece. Moreover, since the gap between the mandrel and the workpiece is set at 5 mm, the wall thickness of the workpiece increases during the first reduction process. However, during the second reduction, the change in model spacing necessitates further reduction of the wall thickness. During this second reduction, friction between the mandrel and the workpiece impedes the axial flow of the internal metal, leading to metal accumulation in the areas that are in
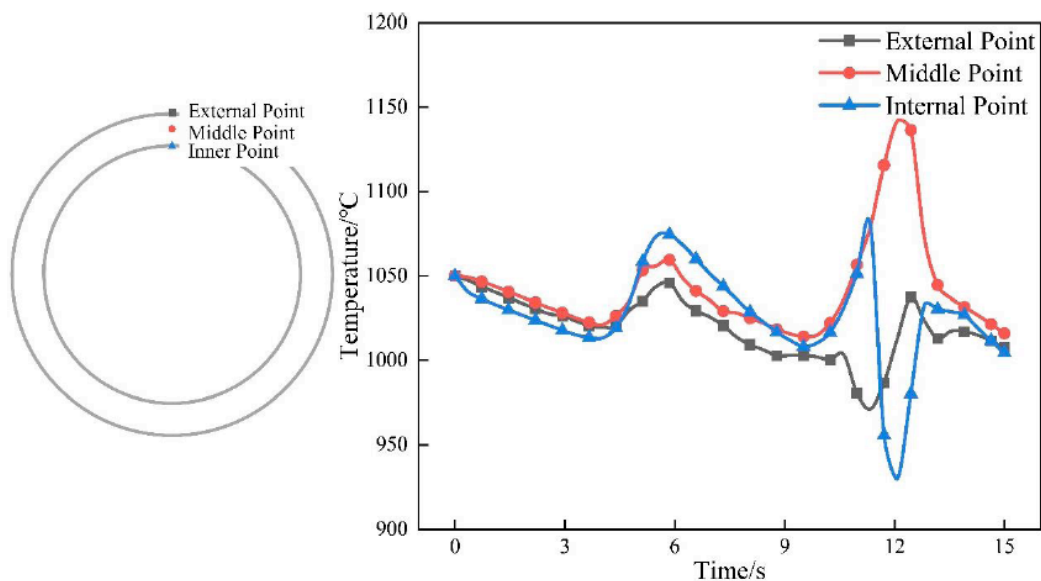

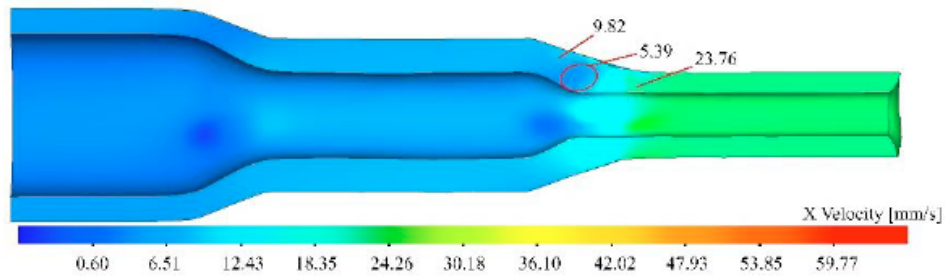**Figure 7:** The temperature change of the selected point of the workpiece.

Figure 8: axial velocity component.

contact with the mandrel. The region highlighted in the circle in Figure **8** indicates that the axial velocity component at this stage is significantly lower than in other areas, further illustrating this phenomenon.

3.2. The Influence of Initial Wall Thickness on Concavity Depth

The concavity depth at the ends of the workpiece significantly increases with a rise in initial wall thickness. This phenomenon occurs because a thicker initial wall allows a greater volume of metal to participate in the deformation process. Following the first reduction rolling, the portions of the piece not constrained by the die enter a stage of free deformation. As the initial wall thickness increases, this free deformation effect exacerbates the concavity at the ends of the workpiece.

In contrast, after undergoing skew tandem rolling, the workpiece with a wall thickness of 4 mm exhibits a relatively uniform distribution of plastic strain after the second reduction, significantly reducing the occurrence of concavity. Conversely, for the other workpieces, the plastic strain in the radial direction shows a decreasing trend after the second reduction. Notably, the workpiece with an initial wall thickness of 10 mm demonstrates the most significant reduction in plastic strain, resulting in the most pronounced concavity depth at its ends. The trend of concavity depth variation is illustrated in Figure **9**.

Research indicates that two effective methods can mitigate the concavity depth issue at the ends of workpieces during the three-roll skew rolling process. First, using hollow tubes with thinner wall thickness can significantly alleviate the concavity phenomenon. Thin-walled hollow tubes distribute deformation stresses more efficiently than their thick-walled counterparts during the rolling process, thereby reducing concavity depth. Second, applying an equal-volume method for chamfering the ends of the workpiece can further help mitigate the concavity issue. Chamfering enhances the geometry of the ends, decreasing the occurrence of concavity and improving

the overall forming quality of the workpiece. The implementation of these two methods offers effective technical solutions for optimizing the three-roll skew rolling process, contributing to higher quality in the forming of aerospace turbine shafts.
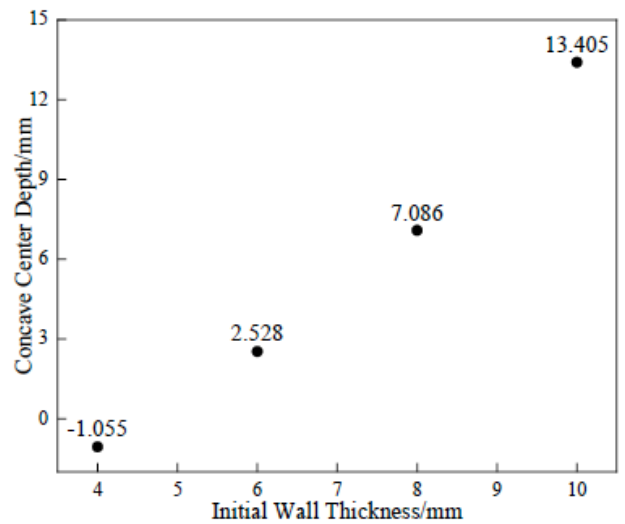

Figure 9: Relationship between concave center depth and initial wall thickness.

CONCLUSIONS

1.   In the process of forming hollow stepped shafts using the skew tandem rolling method, the amount of deformation gradually increases along the rolling direction, reaching its peak after undergoing a second reduction rolling. The stress distribution is primarily concentrated in the contact areas between the rollers and the workpiece, as well as between the mandrel and the workpiece, with the stress levels in the former being significantly higher than those in the latter.

2.   During the rolling process of large cross-sectional reduction, although the presence of the mandrel effectively maintains the inner diameter dimensions of the workpiece, it significantly impacts the temperature variations of the inner wall during the rolling process.

Additionally, it exacerbates the concavity issue at the ends of the workpiece to some extent.

3.   Research indicates that there is a certain relationship between the initial wall thickness and the depth of concavity. As the initial wall thickness increases, the concavity issue becomes more pronounced. This occurs because the increase in wall thickness leads to a gradual reduction in the amount of metal deformation in the radial direction, thereby intensifying the concavity phenomenon at the ends.

ACKNOWLEDGMENTS

REFERENCES

[1]   Wang H Y. Measurement method for coaxiality of low-pressure turbine shafts in aircraft engines based on multi-Bias error separation. Harbin polytechnic institute, 2020.

[2]   Wu H, Kong X W, Luo P. Constitutive equation for high-temperature deformation process of GH4169 Alloy. Mechanical Design and Manufacturing, 2020(8): 163-167.
https://doi.org/10.19356/j.cnki.1001-3997.2020.08.038

[3]   Shanxi Hongyuan Aviation Forging Co., Ltd. An integrated forging method for a large GH4169 turbine shaft: CN201611117336.1. November 16, 2018.

[4]   Tan H, Shi M J, Liu J X, *et al*. Numerical simulation of precision wedge cross-rolling for TC4 axle components with large cross-sectional shrinkage rate. Journal of Weapons Equipment Engineering, 2022; 43(7): 14-19.
https://doi.org/10.11809/bqzbgcxb2022.07.003

[5]   Pater Z, Tomczak J, Bulzak T, *et al*. Numerical and experimental study on forming preforms in a CNC skew rolling mill. Archives of Civil and Mechanical Engineering; 2022; 22(1): 1-21.
https://doi.org/10.1007/s43452-022-00373-0

[6]   Bulzak T, Pater Z, Tomczak J，*et al*. Study of CNC skew rolling of hollow rail axles with a mandrel. Archives of Civil and Mechanical Engineering,2024; 24(3):1-15.
https://doi.org/10.1007/s43452-024-00954-1

[7]   Tomczak J, Pater Z, Bulzak T, *et al*. Design and technological capabilities of a CNC skew rolling mill. Arch Civ Mech Eng 21,72(2021).
https://doi.org/10.1007/s43452-021-00205-7

[8]   Pater Z. A Comparison of two-roll and three-roll cross wedge rolling processes. Advances in Science and Technology Research Journal. 2023; 17(1): 252-266.
https://doi.org/10.12913/22998624/158029

[9]   Shu X D, Xia Y X, Zhang S, *et al*. A Multi-roll inclined continuous rolling forming method for large cross-sectional shrinkage rate step shafts. December 22, 2023.

[10]   Shu X D, Zhang S, Shu C, *et al*. Research and prospect of flexible forming theory and technology of hollow shaft by three-roll skew rolling. International Journal of Advanced Manufacturing Technology, 2022; 123(3-4): 689-707.
https://doi.org/10.1007/s00170-022-10242-y

[11]   Shu, X, Ye C Q, Wang J T, *et al*. Analysis and prospect of precision plastic forming technologies for production of high-speed-train hollow axles. Metals, 2023; 13(1): 145-145.
https://doi.org/10.3390/met13010145

[12]   Xia Y X, Shu X D, Shi J N, *et al*. Forming quality research on the variable-diameter section of the hollow axle in three-roll skew rolling. Materials, 2022; 15(16): 5614.
https://doi.org/10.3390/ma15165614

[13]   Zuo J R, Mei B Z, Zhang S, *et al*. Advancements and development trends in plastic forming technologies of hollow shafts. CAILIAO GONGCHENG-Journal of Materials Engineering, 2024; 52(9): 82-93.
https://doi.org/10.11868/j.issn.1001-4381.2023.000728

[14]   Zhang S, Shu X D, Wang J T, *et al*. The Mechanism of forming hollow shafts with constant wall thickness by three-Roll skew rolling. Metals, 2024; 14(6): 702-702.
https://doi.org/10.3390/met14060702

[15]   Zhang Q D, Zuo J R, Yang C, *et al*. Investigation of deformation behavior and strain-induced precipitations in Al–Zn–Mg–Cu alloys across a wide temperature range. Scientific Reports 14, 14722 (2024).
https://doi.org/10.1038/s41598-024-65669-y

[16]   Zhang, Q D, Zuo J R, Xia Y X, *et al*. Investigation of hot deformation behavior and three-roll skew rolling process for hollow stepped shaft of Al-Zn-Mg-Cu alloy. Journal of materials Research and Technology-JMR&T, 2024; 32: 4106-4121.
https://doi.org/10.1016/j.jmrt.2024.08.183

[17]   Chen C, Shuang Y H, Chen J X, *et al*. Research on a new process for inclined continuous rolling of Titanium alloy seamless tubes. Rare Metal Materials and Engineering, 2023; 52(03): 959-967.
https://doi.org/10.12442/j.issn.1002-185X.20220678

[18]   Chen C, Chen J X, Shuang Y H, *et al*. Short-flow rolling process and heat treatment of seamless Titanium alloy tube. Metals, 2023; 13(3): 527-527.
https://doi.org/10.3390/met13030527

[19]   Chen Q, Shu X D, Li Y M, *et al*. Integrated forming process and numerical simulation and analysis of pierced rolling for aviation engine turbine shafts. Journal of Ningbo University (Natural Science Edition), 2023; 36(06): 24-29.
https://doi.org/10.20098/j.cnki.1001-5132.2023.0517

[20]   Niu X. Research on key process technologies of inclined continuous rolling process. Taiyuan University of Science and Technology, 2016.

[21]   Cao X Q. Study on the flexible inclined rolling forming and microstructural evolution of hollow shafts. University of Science and Technology Beijing, 2023.

[22]   Zhang S. Research on the mechanical behavior and formability synergy control mechanism of three-Roll inclined rolling forming of hollow axles. Ningbo University, 2022.